7 SCIENTIFIC HIGHLIGHT OF THE MONTH

Non-reactive metal-oxide interfaces: from model calculations towards realistic simulations

Jacek Goniakowski[a,b], Christine Mottet[a], and Claudine Noguera[b]

[a] *Centre de Recherche en Matiére Condensée et Nanosciences, CNRS, Campus de Luminy Case 913, 13288 Marseille Cedex 9, France*

[b] *Groupe de Physique des Solides, Universités Paris 6 - 7 and UMR CNRS 7588, 140, rue de Lourmel, 75015 Paris, France*

Abstract

In the last decade two principal factors have stimulated the progressive regain of interest for non-reactive metal/oxide interfaces. On one hand, the efforts invested by the community of model catalysis in analysing the reactivity properties of supported metal nano-clusters have resulted in an abundance of high quality experimental data. They have also risen several precise questions on the direct and indirect role played by the substrate, and have thus reiterated the interrogations concerning the nature of interactions at the metal/oxide interfaces. On the other hand, conceptual improvements of first-principles calculations, such as implementations of various GGA functionals, have added enormously to the reliability of these methods, and have enlarged considerably their field of application. However, most ab initio simulations are sooner or later confronted by the constrains on the computational cost, inherent of this kind of approaches. It concern principally the limited size of systems which can be treated in practice, a factor which turns out to be particularly limiting in realistic studies of interfaces, where the mismatch of lattice parameters is at the origin of incommensurate interface structures, long-range reconstructions, or/and complex structural deformations and dislocations.

In this paper we give an overview of an effective approach to simulate non-reactive deposition of nano-scale metal objects on a surface of highly ionic oxide. The core of this approach is a many-body potential energy surface (PES) constructed on the basis of results of ab initio calculations for model metal/oxide interface structures. We present its application to a study on substrate-induced change of equilibrium atomic structure and morphology of metal nano-clusters, to an analysis of stress release at the interface, and to an investigation of the role of oxide substrate on the melting properties of supported clusters. We end the paper by a brief discussion of defects. Since in the case of highly ionic substrates, surface defects modify strongly the electronic and adhesion properties of the interface, they become often a key ingredient of realistic simulations. At present, more dedicated experimental investigations, supported by model ab initio studies, are still necessary in order to fully access their impact on the observed properties of metal deposits.

1 Introduction

Recent progress of ab initio methods and a continuous improvement of computer performances, enable first-principles simulations on systems of growing complexity and reduce systematically the gap between what can be modelled and what is of direct interest in the real world. On one hand, this concerns a better account of approximations underlying the existing ab initio approaches and aims at a more reliable description of the electronic interactions in, and beyond, the electronic ground state. On the other hand, the concern is focused on the structural and chemical complexity of simulated systems and aims directly at a more realistic representation of the experimental conditions.

1.1 Realistic simulations on large systems

Very often, a relatively large number of independent degrees of freedom needs to be taken into account in order to obtain a satisfactory structural model of a large-cell reconstruction, a dislocation, or a complex grain boundary. The very same issue of calculation size reappears somewhat differently in simulations which tackle the effects of finite temperature, where the computational effort is related to the length of calculated temporal evolution of the system. For the latter, statistical averages need to be performed over series of configurations (electronic, atomic, compositional, etc.) and the convergence with respect to their number may, quite obviously, represent a challenge even for a system of a moderate number of particles. It is worth keeping in mind that in the case of a large system, a seemingly simple task of searching for a structural ground state gives often rise to similar computational problems. In most cases, an efficient treatment of both classes of problems requires adequate tools, such as molecular dynamics or Monte Carlo simulations. Depending upon the problem, the generated series of configurations are used to minimize the potential energy, to evaluate thermodynamic averages, or to follow the trajectory of the system.

There exist several cases where ab initio techniques were successfully applied to large/dynamic simulations. In fact, the Car-Parrinello[1] pseudopotential plane wave technique was designed to carry out first-principle molecular dynamics simulations on the fly, and is particularly useful for an efficient exploration of atomic trajectories in an insulating or semi-conducting system. However, it is much less well suited for Monte Carlo simulations, and its direct use for dynamic simulations remains of limited use, either because the pseudopotential method is computationally too demanding (for atoms like transition metal atoms or oxygen, which require a high energy cut-off), or because the number of atoms/configurations that can be explicitly treated remains not large enough. As an example, most of prototype systems considered in the field of model catalysis require a full structural optimization of a supported, late transition metal cluster of a few tens/hundreds of atoms. Such a task remains at present by far out of the reach of ab initio calculations.

An alternative approach consists in using the first-principle calculations to parametrize an energetic model, which is then coupled to an adequate statistical method. Depending on the problem, its complexity may range from a mere estimation of energies of selected configurations or activation barriers, to a full parametrization of a set of effective inter-atomic potentials.

Whereas similar in spirit to various existing semi-empirical methods, this approach is limited neither by the existing experimental data, nor by the transferability of the information which can be deduced from the experiments. This is particularly important for systems where the latter is insufficient or difficult to extract from the complex experimental results. In this domain, the first principles calculations offer the unique possibility of tailoring the model systems, at and beyond the structural ground sate, in view of extracting the necessary information. The present study on metal/MgO(100) interfaces is an example of application of this latter strategy.

1.2 Case of non-reactive metal-oxide interfaces

Although systems involving non-reactive metal-oxide interfaces may appear simple compared to those where inter-diffusion or oxidation takes place, their difficulty resides in the not yet fully understood microscopic nature of interactions responsible for the adhesion at the interface cohesion, and in particular, of mechanisms which drive the structural, electronic and growth characteristics of metal deposits. For metals at the end of the transition series, which are the most interesting for their applications in catalysis, this difficulty is enhanced by the overall weakness of interactions at the interface. In these cases, the chemical bonding is often assumed to be negligible, and the adhesion is assigned principally to the van der Waals and image charge contributions. However, no rigorous estimation of the relative strength of these contributions has yet been proposed [2, 3, 4, 5, 6, 7, 8].

Due to the weakness and complex character of interactions at the interface, the applicability of the state-of-the-art first-principles techniques has also been questioned. Whereas the concern is often focused principally on the van der Waals contribution, the method-dependent degree of localization of valence electronic density may contribute to imprecisions in estimation of the image charge effects as well. Presently, after a decade of systematic comparisons with high quality experimental results, we are confident that *ab initio* calculations predict the correct preferential adsorption geometries and give a correct estimation of principal features of adsorption energetic. However, since the comparison of electronic or precise energetic characteristics of the interface is much more challenging the complete microscopic description is still far from being settled.

As a model highly ionic substrate, the MgO(100) surface is probably the most studied oxide surface and constitutes one of the most widely used oxide substrates. From the experimental point of view, its low reactivity, weak tendency to deviate form stoichiometry or to oxidise the deposited metal, are accompanied by a relative easiness of preparation of mono-crystalline samples with large terraces and limited number of defects. Its wide gap and its strong ionicity minimize the effects due to interface electron transfers, but are at the origin of strong electrostatic field which polarizes the metal at the interface. The weakness of interactions at the interface limits the extent of the reciprocal influence of one material upon the other. Although the distortion of the metal electronic structure by the substrate electrostatic field can be quite significant, from the point of view of interface cohesion or interactions within the metal itself, this effect seem to have only a secondary importance. This, together with the rigidity of the crystalline structure and the resulting relatively simple atomic structure of the metal/MgO interface, privileged approaches based on a potential energy surface as probably the most efficient tool for large scale simulation.

2 Model ab initio calculations

In order to get an insight into the basic microscopic mechanisms that drive the adhesion properties of a metal/MgO(100) interface, we have performed DFT calculations (within full-potential LMTO [9] and LAPW [10] methods and both LDA and GGA [11] functionals for the exchange-correlation energy) for a series of model systems, chosen as to shed light on the relevant factors. In the following, with a set of chosen examples, we focus on the characteristics specific to the highly ionic substrate (MgO), and emphasize their relationship to the interface atomic structure and adhesion energetics. Further on, in a more general context, we discuss trends in the series of transition metals.

2.1 Choice of model systems

One of the advantages of first principle calculations resides in the fact that the quality of results does not depend directly on the proximity to the structural ground state. In fact, contrary to methods with adjustable parameters, which work the best in the direct proximity of the adjustment conditions, first principle approaches describe equally well any reasonably chosen system. This concerns in particular the atomic structures and chemical compositions which, due to their elevated total energy, could never be observed experimentally. This aspect, which at first glance may seem somewhat academic, enables, by an adequate choice of model systems, a quasi-direct access to selected aspects of the problem. It is also essential for construction of effective interactions, such as potential energy surface (PES) methods, for which the energetics of configuration far from structural equilibrium needs also to be assessed.

In the present case of metal deposited on an oxide substrate, due to the mismatch between oxide and metal lattice parameters, the energetic and electronic characteristics of a realistic interface are a complex mixture of these corresponding to various local interface structures. The big advantage of the model calculations is to enable a quasi-independent treatment of the different components and contributions, by fixing selected structural degrees of freedom. The essential drawback of this procedure is the additional constrain on the lattice parameter of the deposited metal, necessary to assure the matching of the two lattices at the interface. Its effect is partially compensated by a tetragonal distortion of the metal lattice, which acts towards a conservation of the atomic volume. Although necessary in order to reduce the size of the system and to make it treatable on ab initio level, it is clear that this procedure may lead to non-negligible errors in the case of interfaces with large lattice mismatch.

Due to the simplicity of the MgO(100) surface, once a pseudomorphic structure of the interface is assumed, three factors only are necessary to characterize the essential features of the local atomic structure at the interface.

1. The relative position of the deposited metal atoms with respect to ions of the substrate. The continuum of possibilities can be spanned by three high-symmetry adsorption geometries: metal atoms on-top surface oxygen, on-top surface magnesium, or in intermediate (hollow) adsorption sites.

2. The coverage of the surface. Since it is relatively well established that the cohesion in

metallic system does not have a pair-wise character, it is necessary to investigate to what extent local atomic environment in the metal influences the metal-oxide interaction. Three model cases span the principal coverage-dependent effects: adsorption of an isolated metal atom (in the periodic calculations represented by 0.25 ML or less), deposition of a full metal mono-layer (one metal atom per substrate adsorption site), and an interface between MgO and a thicker metal deposit (2ML or more).

3. The interface separation d_{sep} between the metal deposit and the substrate. Whereas the parameter of first interest is often the optimal interface separation for which the total energy is minimal, one needs to remember that at a realistic interface an important number of atoms is located off their preferential adsorption site and/or at distances different from those estimated in model calculations. This is why the PES needs to also account for the whole spectrum of d_{sep}.

In the presentation that follows we freely benefited of the above advantages of ab initio calculations, and we chose the model examples which more clearly reveal the effects under consideration.

2.2 Electronic structure of the interface

The physics of metal-insulator interfaces largely relies on the nature of interface electronic states close to the Fermi level, which drives the value of the interface dipole moment, and the band alignment at the interface. The best known and the most often referred states in phenomenological models of interface, the Metal Induced Gap States (MIGS) result from the matching of delocalized metal wave functions with exponentially decaying insulator states in the gap energy range. On the other hand, "polarization" states result from strong distortions of the metal valence band by the electrostatic field of the substrate. They are specific to strongly ionic substrates and are responsible for image charge effects. Finally, bonding and anti-bonding interface states refer to chemical bonds across the interface, which appear at well-defined energies, and not only in the insulator band gap energy range. They have often been neglected, especially at weakly adhesive interfaces.

2.2.1 Metal-oxygen bonds across the interface

Formation of an interface chemical bond between oxygen and metal orbitals is at the origin of appearance of bonding (B) and anti-bonding (AB) states located respectively at and below the oxide valence band and above the metal band. They are associated to an enhancement or depletion of the electronic density at the interface, respectively. Although this precise criterion cannot be unambiguously estimated due to the complex deformation of dispersive bands, any occupied state whose energy is lowered during the interface formation enhances the adhesion, the opposite being true for the states pushed upwards on the energy scale. The position of the Fermi level within the AB band is decisive: a fully occupied AB band always overcompensates the cohesive contribution of its B counterpart.

Presence of interface metal-oxygen bonding can be detected even when late transition metals are involved. For example, at the Pd/MgO(100) interface, Fig. 1, the hybridization between

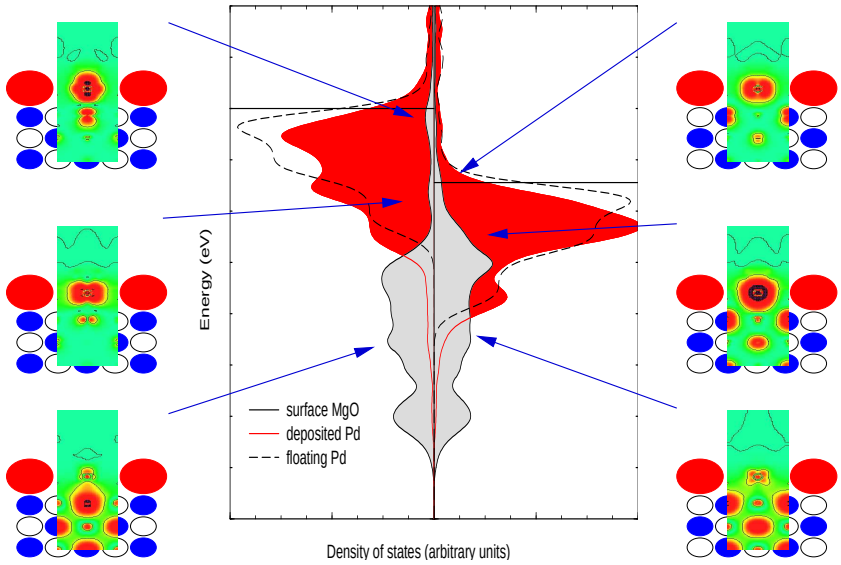

Figure 1: Pd/MgO(100) interface. Metal-oxygen bonds are traced in the local density of states calculated for a Pd monolayer at oxygen (left panel) and magnesium (right panel) adsorption sites, for fixed interface separation of 2.37 Å. Projections on the surface oxide valence band (grey) and on the palladium band (red) are explicitly plotted. The energy scales are aligned by the core levels of oxygen ions in the slab center. LDOS of an unsupported Pd layer (dashed line) with the same lattice parameters and the same Fermi level is plotted as a reference. Side panels present the corresponding maps of the electron density in the plane perpendicular to the interface, calculated in energy windows of 1 eV centered at LDOS features indicated by the arrows. The presented maps are centered on the oxygen (magnesium) ion. Colours red and yellow depict the regions of elevated electron density, whereas green corresponds to zero. From [12].

oxygen and palladium orbitals is clearly visible: interface Pd-O states can be detected below the Pd band, and within the MgO band gap. Among the latter, some contribute to a featureless LDOS in the whole MgO gap (they correspond to MIGS and will be discussed in Sec. 2.2.3), while others are at well-defined energies and represent the AB states of the Pd-O bond. Due to the different spatial orientation of the atomic orbitals involved in the bond formation, their energy and their character are strongly geometry dependent.

In the case of Pd atoms on-top of surface oxygen, the interaction mainly involves the O p_z and the Pd $d_{3z^2-r^2}+sp$ orbitals, whose shape is clearly visible in the electron density maps. The relatively well pronounced splitting of the B and AB contributions is due to strong spatial overlap of the two orbitals. It results in a partial depopulation of the AB component and contributes directly to the cohesion of the interface.

When adsorption takes place on-top magnesium, due to the core-core repulsion between palladium and surface magnesium, the overlap between Pd and O orbitals is smaller. It is not fully compensated by a smaller separation between the Pd and O bands on the energy scale and, although present in this adsorption geometry, the Pd-O bonding gives only a negligible contribution to adhesion.

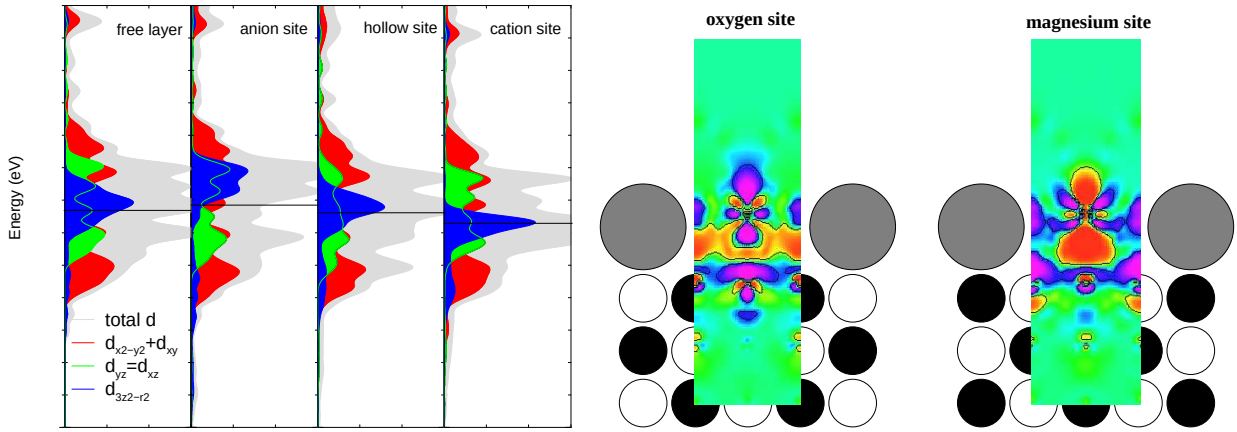

Figure 2: Mo/MgO(100) interface: polarization of the Mo layer by the MgO electrostatic field. Left panel presents the Mo LDOS decomposition (total (grey), $d_{x^2-y^2} + d_{xy}$ (red), $d_{yz} = d_{xz}$ (green), and $d_{3z^2-r^2}$ (blue)), obtained for an unsupported, strained Mo layer, and for the same layer deposited in three alternative adsorption geometries. The energy scales are aligned by the oxygen core levels in the center of the slab, except for DOS of the free layer, whose Fermi level is aligned to that of Mo at the hollow site. Right panel presents maps of differential electron density (difference between the density of constituted interface and the sum of separate systems), plotted in the plane perpendicular to the interface and centered on surface oxygen (oxygen adsorption site) or surface magnesium (magnesium adsorption site). Red and yellow colours correspond to an enhancement of electron density, whereas blue and violet represent a reduction. From [13].

2.2.2 Polarization by the substrate electrostatic field

Additionally to metal-oxygen hybridization, the metal valence band is polarized by the electrostatic field of the substrate. Indeed, an upward (downward) shift of metal orbital energies is systematically registered when adsorption takes place on top oxygen (magnesium) sites. However, due to the different spatial orientation of the different components of the d band with respect to the substrate electrostatic field, this shift is strongly non-uniform and produces a crystal-field-like distortion of the metal band. As a consequence, it modifies the positions of orbitals with respect to the Fermi level and is accompanied by an electron redistribution between the different components. This process does not involve any charge transfer across the interface, and corresponds thus to a substrate-induced polarization of the metal interface layers.

We illustrate this effect on the Mo/MgO(100) interface, Fig. 2. Due to its angular orientation, the largest shift concerns the $d_{3z^2-r^2}$ orbital, whose lobe points towards the substrate. With respect to its relative energy in the unsupported monolayer, it is shifted upwards (and above the Fermi level) when above the surface anion and downwards (and partially below the Fermi level) above the surface cation, whereas its position is only little modified in the surface hollow site. For orbitals with lobes in the plane of the metal layer ($d_{x^2-y^2} + d_{xy}$) the displacement with respect to the Fermi level is much smaller. As shown in the maps of differential electron density, Fig. 2, this non-uniform shift is accompanied by an electron redistribution among the components of the metal d band. Namely, above oxygen the $d_{3z^2-r^2}$ component transfers its electrons to the other d orbitals, the opposite being true for adsorption above cations. By emptying the space

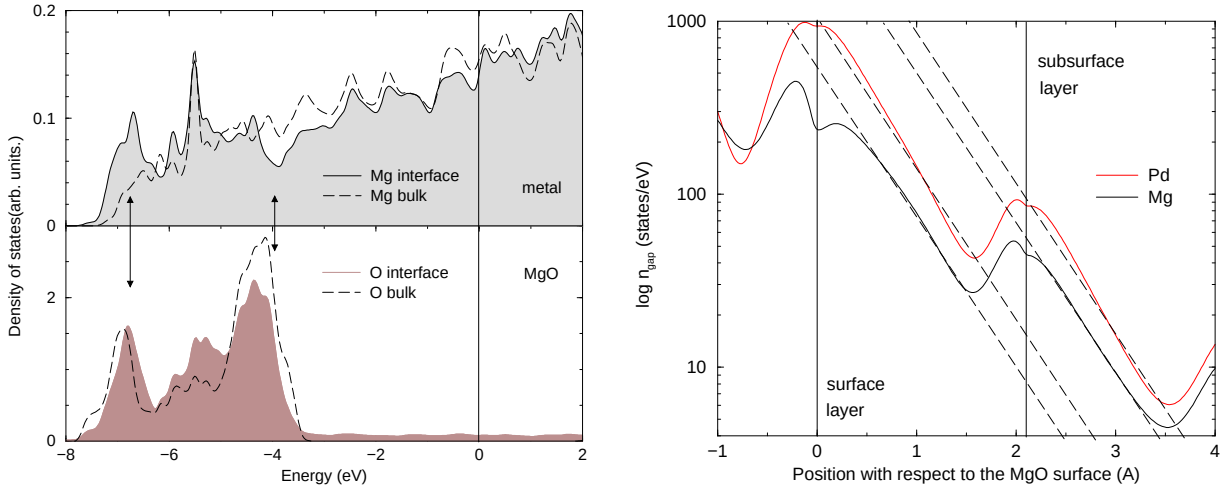

Figure 3: Conventional MIGS: Left panel presents the LDOS of Mg multilayers deposited on the MgO surface. Although, with respect to the bulk DOS (dashed lines), the deformation of interfacial oxygen and magnesium bands is clearly visible (cf. zones marked with arrows), it does not give rise to localised states in the gap region. The structureless continuum of gaps states visible in the LDOS of interface oxygen corresponds to the conventional MIGS. Their penetration into the oxide is exemplified by the electron density n_{gap} (obtained by integrating states between the bulk MgO VBM and the Fermi level), plotted as a function of the coordinate perpendicular to the interface (full black line in the right panel). An equivalent plot for the Pd/MgO(100) interface is also given (full red line). Note the logarithmic scale for n_{gap}. From [14].

above surface oxygen and by populating that above surface magnesium, this process mimics the macroscopic "image charge" effect.

2.2.3 Conventional MIGS

Conventional MIGS, which are produced by the exponential decay of delocalized metal states within the insulator, are also present at metal/oxide interface. This is also true for interfaces with small or absent chemical bonding, in which cases MIGS produce a structureless continuum of states above the substrate VBM. Their decay within the oxide, which can be characterized by their penetration length, is determined principally by the nature of the oxide and nearly independent of the metal [14], in agreement with the MIGS theory developed in Ref. [15]. On the other hand, the MIGS density of states at the interface is strongly metal-dependent.

Presence of MIGS can be detected at the Pd/MgO(100) interface, Fig. 1, where however they coexist with more localized bands due to Pd-O bonds. At the Mg/MgO(100) interface, Fig. 3, the Mg-O chemical bonding is weak, the deformation of interfacial bands is less pronounced, and the Mg-induced MIGS in the MgO band gap are practically structureless. Aside from oscillations on the MgO cores, they display a clear exponential decay, characterized by a penetration length $l_p \sim 0.5$ Å.

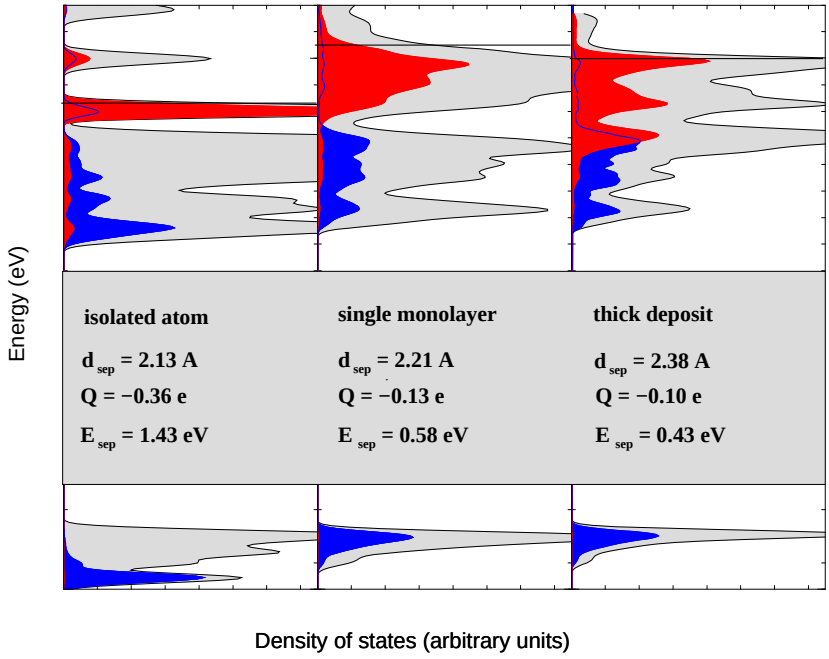

Figure 4: LDOS at a Pd/MgO(100) interface as a function of Pd coverage: an isolated Pd atom (0.25 ML), a single Pd monolayer, and a thicker (5ML) Pd deposit. Are given: total and projected DOS (total (gray), surface oxygen (blue), and palladium (red); energy scales are aligned by the core levels of bulk oxygen ions), equilibrium interface separation d_{sep} (Å), interface charge transfer (electron/oxygen adsorption site, negative sign corresponds to electrons transferred from the substrate towards deposited metal), and separation energy E_{sep} (eV/oxygen adsorption site) defined as a difference of total energy between constituted metal/oxide system and its two separated components: clean MgO(100) slab and floating (strained) metal layer. From [16].

2.3 Dependence on the metal coverage

Whereas it is relatively well established that cohesive interactions in transition metal and transition metal compounds do not have a pair-wise character (see Sec. 3.1), the interactions at metal/oxide interfaces, and their relation to the local environment of the deposited metal atoms is not entirely elucidated. One of the difficulties resides in the fact that, as a function of metal coverage, the various contributions (van der Waals, image charge, and chemical bonding) do not behave in the same way.

Considering again the Pd/MgO(100) interface in its ground state atomic configuration (palladium atoms on-top surface oxygen), we illustrate the strong dependence on the metal coverage by considering three adsorption models, Fig. 4. The metal-oxide interaction is clearly the strongest in the limit of isolated adatoms and weakens progressively with increasing Pd coverage, as shown by the variation of E_{sep}. The decrease of E_{sep} is accompanied by an expected increase of the equilibrium interface separations d_{sep} and by a weakening of the interface electron transfer.

The origin of this evolution can be traced back to the changes of hybridization between oxygen and Pd orbitals at the interface [17]. At low coverages, the Pd LDOS is narrow and located close to the MgO VBM. The coupling is strong, the splitting of bonding and antibonding states is well

pronounced: the B component is below the bulk O $2p$ band, and the AB component is partially depopulated. This corresponds to an important electron transfer across the interface. At higher Pd coverages the width of the Pd band increases progressively and so does the separation between Fermi level (fixed mainly by the Pd band) and the MgO VBM. Hybridization between palladium and oxygen orbitals is thus weaker and, taking into account the increasing width of the Pd band, more and more inefficient to push the AB band above the Fermi level. This progressively reduces the related gain of energy and the interface electron transfer.

The correlation between the changes of Pd-O hybridization and E_{sep} points out to the chemical bonding as the dominant contribution to the separation energy in the Pd/MgO(100) system. Whereas such a behaviour may indeed be expected at interfaces where adhesion is dominated by chemical bonding, it is worth mentioning that this is not the general trend. In fact, at weakly adhesive interfaces, the behaviour is rather determined by van der Waals and image charge contributions. Additionally, also the relative weight of the various contributions may also vary as a function of coverage. This is the case at Ag/MgO(100) interfaces, where the evolution of $E_{\rm sep}$ is opposite to that of Pd/MgO(100), and dependent on the precise choice of the exchange-correlation functional [18, 19].

2.4 General trends along the transition series

In order to generalize the preceding approach and to put it in a wider context, in Fig. 5 we present the evolution of interface characteristics for metals along two transition series.

The general trends are the following:

- The interface ground state always corresponds to adsorption above oxygen. This trend is relatively strong at the beginning and in the middle of the series, where in addition, due to the core-core repulsion, no (meta)stable adsorption takes place above magnesium sites.
- The separation energy E_{sep} displays a well pronounced decrease in the second half of the series (oxygen site). This trend is mainly ascribed to changes in the interface metal-oxygen bonding. Indeed, following the arguments of Sec. 2.2.1, we observe in Fig. 5 a progressive filling of the Me $d_{3z^2-r^2}$ -O p_z AB component and a strong polarization of the metal layer by the electrostatic field of the substrate. The electron redistribution between the different d orbitals contributes also to a weakening of metal cohesion of the deposited layer, and thus to an additional weakening of the separation energy.
- For the metals of the very end of the transition series (Ag, Cu), the sp character of the electronic states close to Fermi energy is associated to a considerably smaller separation energy. The contribution due to the formation of interface bonds is smaller and the part of image charge and van der Waals interactions is likely more important.

3 Calculations on large systems

If the DFT-based methods have proved their usefulness for treating model metal/oxide interfaces, the computational effort needed for a realistic treatment of large-size systems limits considerably

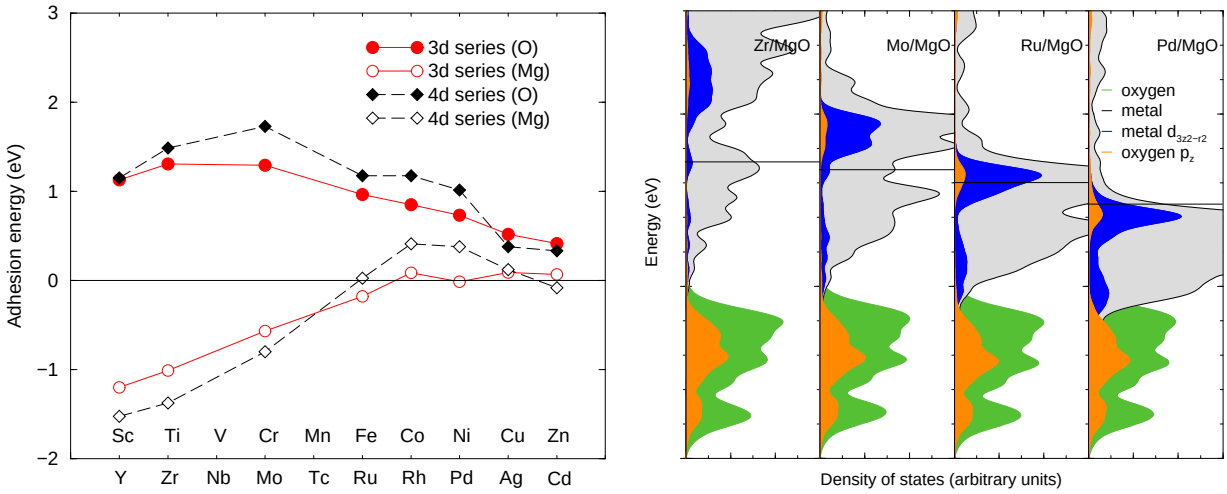

Figure 5: Interface characteristics as a function of the deposited metal. Left panel presents the separation energies for deposition of $3d$ (red circles) and $4d$ (black squares) transition metal monolayers on the oxygen (full symbols) and magnesium (empty symbols) sites of the MgO(100) surface. For sake of a direct comparison, all energies correspond to fixed interface separations: $d_{sep} = 2.4$ Å (oxygen adsorption site) and $d_{sep} = 2.6$ Å (magnesium adsorption site). Relaxation of this constrain does not modify the depicted tendency. Right panel gives the interface LDOS: transition metal band (grey) and its $d_{3z^2-r^2}$ component (blue), oxygen band (green), and its p_z component (yellow), for Zr, Mo, Ru, and Pd monolayers deposited on the oxygen sites of the MgO(100) surface. Energy scales are aligned by the core levels of bulk oxygen atoms. Effects due to spin-polarization are not taken into account. From [13, 20].

their field of application. In particular, it is not yet possible to use them directly for modelling the complex interfaces involving inhomogeneous relaxations, large cell reconstructions, dislocation networks, etc. which have been experimentally observed. This drawback is particularly constraining in modelling of nano-cluster structures, which usually require an extensive search in configurational space. On the other hand, because many fundamental questions on the character of interfacial interactions remain unanswered, there exists no straightforward and reliable semi-empirical methods for modelling these systems. For these reasons, several effective approaches, derived from first principles methods, have been proposed these last years in order to treat metal/MgO interactions [21, 22, 23, 24, 25].

As a model catalyst, Pd clusters supported on MgO(100) have been the subject of many detailed experimental and theoretical studies. Understanding the cluster morphology, the relation between their size and detailed atomic structure, and their interaction with the oxide substrate is a necessary step towards the control of their reactivity. In the following, we describe the Potential Energy Surface approach we have applied to study Pd clusters on MgO(100) [25].

3.1 Second Moment Approximation for the Pd-Pd interactions

Since the cohesion of transition and noble metals is governed by the characteristics of the metal d band [26], several successful semi-empirical approaches have been conceived in order to rationalize the dependence of the cohesive energy on the local environment (coordination) of metal

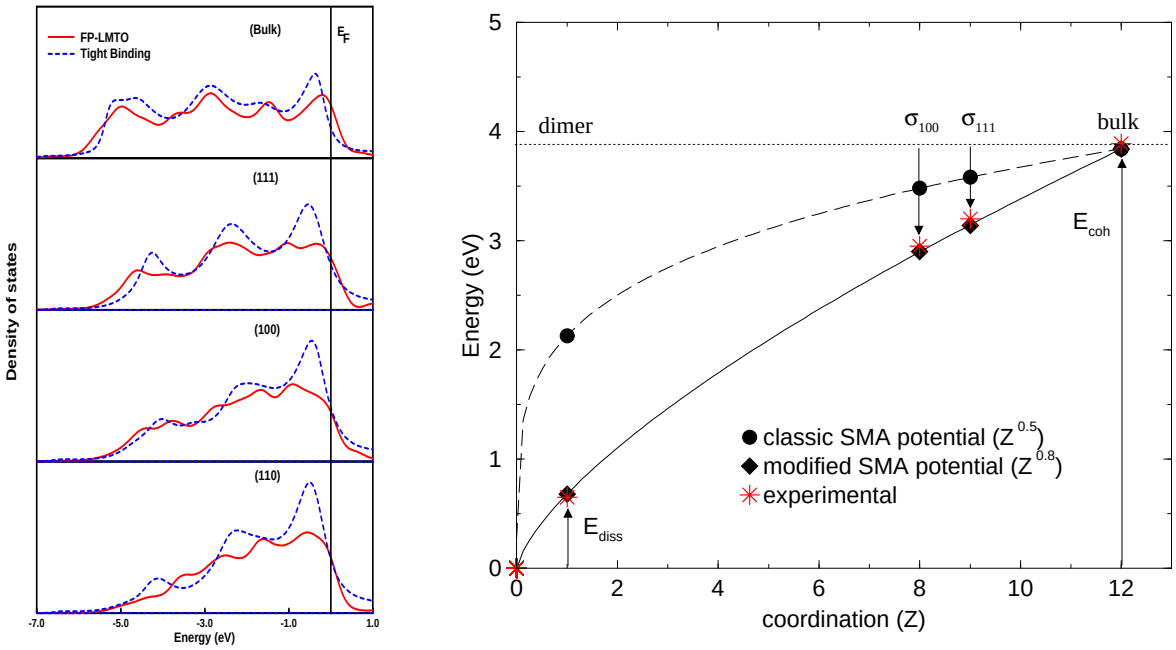

Figure 6: Adjustment of the Pd-Pd potential. Left panel gives LDOS for bulk Pd and for surface Pd atoms at three low index surfaces: (111), (100), and (110). Results obtained within tight-binding calculations with $sp-d$ hybridization based on the charge neutrality per orbital (dashed blue lines) are compared to results of ab initio FP-LMTO calculations (solid red line) [27]. Right panel displays a schematic representation of site energies (E) of Pd atoms as a function of their coordination (Z) obtained within the classic ($E_b \sim Z^{0.5}$: dashed line) and modified ($E_b \sim Z^{0.8}$: solid line) SMA approach. Experimental values of bulk cohesive energy (E_{coh}), surface energies (σ_{111} and σ_{100}), and Pd dimer dissociation energy (E_{diss}) are plotted with red stares.

atoms.

In the so-called second moment approximation (SMA) [28], the attractive part (E_b) of the potential is fitted to the band energy, assuming a rectangular density of states of the same second moment μ_2 as the actual one: $E_b \sim \mu_2^{1/2}$. Moreover, since in the tight-binding approximation, μ_2 is known to be linear in the effective first neighbour coordination number Z, one obtains the usual square-root many-body character of this potential $E_b^{TB} \sim Z^{1/2}$. However, in spite of its overall success, this potential fails to reproduce accurately the experimental variation of the energy as a function of the coordination number in the whole Z-range. The surface energy is generally slightly underestimated [29] and the deviation increases with decreasing Z. This is for example the case for Pd [30].

The alternative is thus either to go beyond the second moment approximation and account for details of the LDOS, or to stay within such an approximation but calculate the second moment as accurately as possible. In both cases this requires to go beyond the tight-binding d-band approximation and an adequate introduction of the $sp-d$ hybridization in tight binding approach. Results of a successful implementation, based on the charge neutrality condition derived from ab initio calculations [27], are illustrated by matching of tight-binding and FP-LMTO densities of states projected at atomic sites of different coordination, Fig. 6. The first

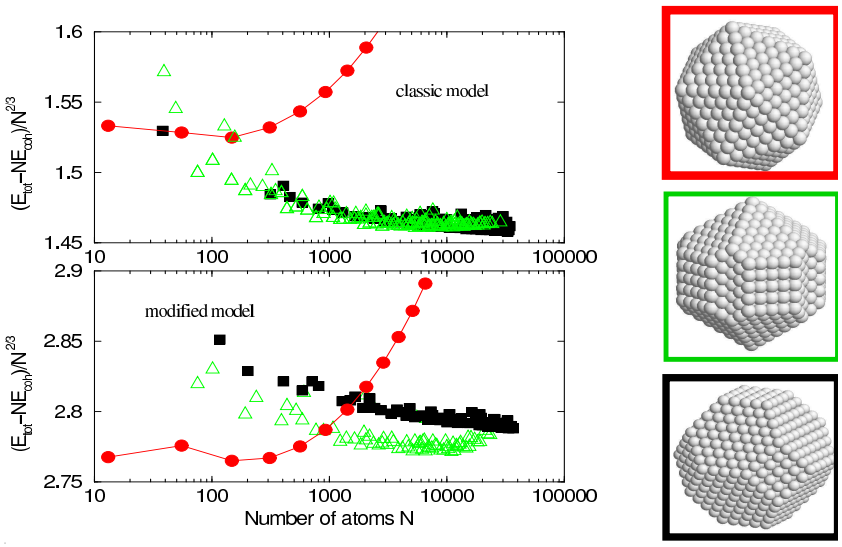

Figure 7: Stability of free Pd clusters: excess energy $((E_{tot}(N) - N.E_{coh})/N^{2/3})$ with respect to bulk Pd cohesion energy $((E_{coh})$ is plotted as a function of cluster size (N) for icosahedron (red circles), decahedron (green triangles), and truncated fcc polyhedron (black squares) cluster structures. Results of both classic (top panel) [34] and modified (bottom panel) SMA approaches are given.

solution, without $sp-d$ hybridization, yields $E_b^{TB} \sim Z^{2/3}$ [31], or to $E^{TB} \sim Z^{4/3}$ when taking this hybridization into account [32]. In second solution, with μ_2 derived either from FP-LMTO results or from tight binding calculations with $sp-d$ hybridization (see Fig. 6) ($\mu_2^{LMTO} \sim Z^{3/2}$), one obtains $E_b^{LMTO} \sim Z^{3/4}$. The proper treatment of $sp-d$ hybridization thus leads to a dependence of the band term which is intermediate between square-root and pairwise. This result seems to be confirmed in the particular case of Pd, for which the experimental variation of the energy with coordination number is found to be almost pairwise. The best account for the experimental data is obtained $Z^{0.8}$ dependence on the coordination number, Fig. 6.

SMA potentials have been used to determine the size range of stability of icosahedral and decahedral structures of free transition and noble metal clusters [33]. The case of Pd, within both classic ($E_b \sim Z^{0.5}$) and modified ($E_b \sim Z^{0.8}$), is illustrated in Fig. 7. For the fcc structures, the excess energy (with respect to bulk cohesion energy) converges monotonically towards a constant value proportional to an average surface energy. For icosahedral and decahedral structures it initially decreases, reaches a minimum, and finally, due to the elastic strain induced in the cluster core by the fivefold symmetry, it diverges at large cluster sizes. Indeed, whereas at small sizes these quasi-periodic structures minimize the surface energy, as the size increases the energy gain due to minimization of surface energy compensates less efficiently the energy of core distortion. Within the modified SMA potential, the critical size increases significantly for both icosahedron to decahedron (from 100 to 1000 atoms) and decahedron to truncated fcc octahedron (from 10000 to 20000 atoms) transitions. This difference is principally due to the increase of the energy of defects (see Fig. 6), which favours cluster structures of minimal surface energy. As a consequence, the stability of quasi-periodic structures is extended towards larger sizes.

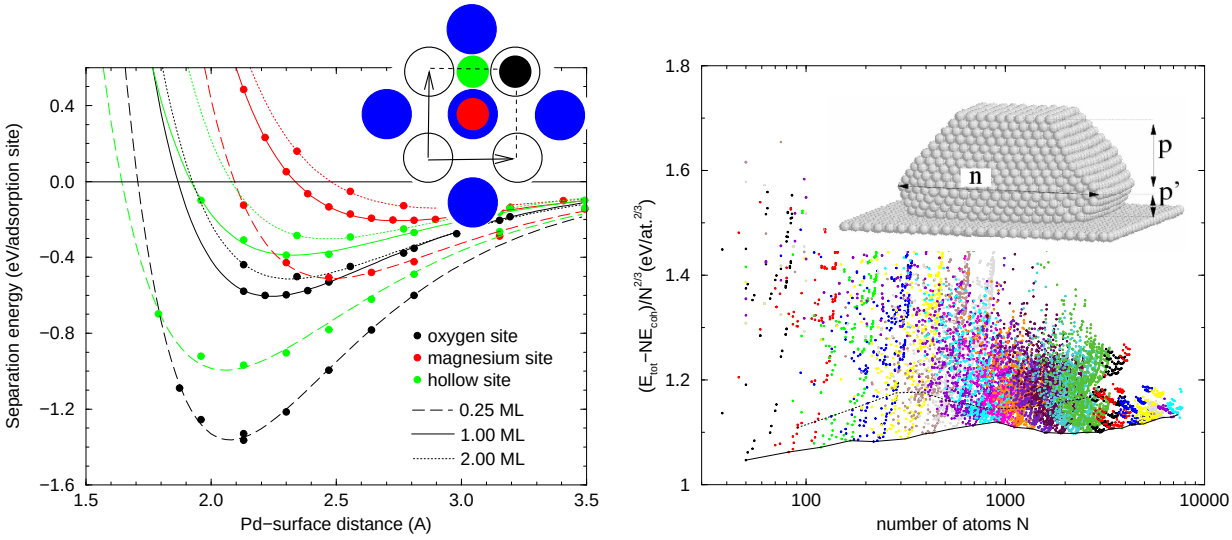

Figure 8: Left panel: adjustment of the Pd-MgO(100) Potential Energy Surface. Circles represent the separation energies (E_{sep}) issued from ab initio calculations, lines correspond to the fitted potential. Oxygen (black), magnesium (red), and hollow (green) sites are considered (see the inset for a schematic representation of the MgO(100 surface) at Pd coverage of 0.25 ML (dashed lines), 1 ML (solid lines), and 2 ML (dotted lines). Right panel: excess energy (see Fig. 7) plotted as a function of cluster size (number of atoms) for Pd clusters supported on MgO(100). Various cluster morphologies have been considered, as defined by parameters depicted in the inset. The doted line corresponds to perfect pyramidal shape and the full line corresponds to minimum potential energy, i.e. the equilibrium cluster morphology. From [35].

3.2 Many-body Potential Energy Surface for Pd-MgO(100) interactions

We derived the many-body potential energy surface representing Pd-MgO(100) interaction, which supplements the SMA Pd-Pd interaction from model DFT calculations, as to take into account the main energetic characteristics described in Section 2. Sites on-top oxygen are energetically the most favourable for Pd adsorption (minima), while magnesium and hollow sites represent respectively maxima and saddle points of the potential energy surface. In addition, the Pd-MgO interaction depends upon the Pd coverage: it is the strongest for isolated ad-atoms and decreases progressively as the number Z of Pd-Pd bonds grows. This ingredient is particularly important in the case of small clusters, characterized by a large proportion of under-coordinated atoms.

The Pd/MgO interaction is assumed to be additive with respect to the number N of Pd atoms: $E^{Pd-MgO} = \sum_{i=1}^{N} E(x_i, y_i, z_i, Z_i)$. It depends on their lateral position (x_i, y_i) with respect to the MgO lattice, on their elevation z_i above the MgO surface, and on the number Z_i of their nearest Pd neighbours. $E(x_i, y_i, z_i, Z_i)$ assures an analytical interpolation between the ab initio results obtained for model interface structures described in Section 2.1. The non-linear dependence of E^{Pd-MgO} on the coordination number Z confers to the fitted PES an effective many-body character. Results of ab initio calculations and the fitted dependence are depicted in Fig. 8.

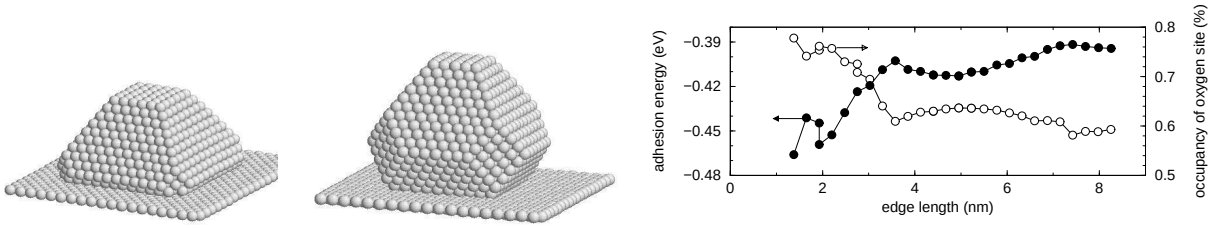

Figure 9: Pd clusters supported on the MgO(100) surface: typical cluster morphologies obtained within the classic (left) and modified (right) SMA potentials. Right panel displays the evolution of the adhesion energy (black dots) and of the average occupancy of oxygen adsorption sites (open circles) as a function of cluster size. From [25].

3.3 Morphology of supported Pd clusters

Structure and morphology of free metallic clusters described in Section 3.1 are modified by the interaction with the substrate. Indeed, experiments on MgO(100) supported Pd clusters have revealed the truncated fcc octahedron structure already at very small cluster size (less than 2 nm) [36]. Following this experimental indication we have focused on clusters of different sizes (edge length) and morphologies (aspect ratio, corner truncations) under the constraint of [100]Pd//[100]MgO epitaxy relation. For each of them, a series of quenched molecular dynamics runs, of different lengths, at various temperatures and initial conditions has been performed (a few nanoseconds of MD runs per cluster), in order to find the potential energy minimum. Typical results are given in Fig. 8.

The most stable clusters have the shape of "flattened" pyramids with truncated edges. Their aspect ratio varies from 0.5 (classic SMA potential)[25] to about 0.75 (modified SMA potential), Fig. 9, in a nice agreement with the Wulff-Kaishew or Winterbottom argument relying on the ratio between metal surface energy and interface adhesion (in analogy to the Young-Dupré equation in case of a liquid droplet wetting a surface). Indeed, the increase of aspect ratio can be directly related to the higher energy of the Pd(100) surface in the modified SMA approach, in good agreement with experimental observations on larger clusters [36].

Whereas for larger clusters, their morphology does practically not depend on cluster size, the smaller ones (less than 4 nm) are subject to detectable structure changes, induced by the variations of interface adhesion energy, Fig. 9. The latter is driven by the Pd-MgO interaction, and thus follows closely the changes of average occupancy of the preferential (oxygen) adsorption site. If small clusters adhere stronger to the MgO(100) surface, it is due to the strain of their structures, which accommodates the lattice mismatch at the interface.

3.4 Substrate induced stress and dislocations

Due to the lattice mismatch between Pd and MgO ($a_{Pd} \sim 0.92 a_{MgO}$) the substrate induces a tetragonal distortion of small clusters, with a dilation in the interface plane and a contraction in the direction perpendicular to the interface, Fig. 10 (A). As the cluster size increases, the energy gain due to the interface adhesion is no longer sufficient to compensate the elastic energy due to strain induced by the lattice mismatch. At about 5 nm, rows of Pd atoms leave their preferential

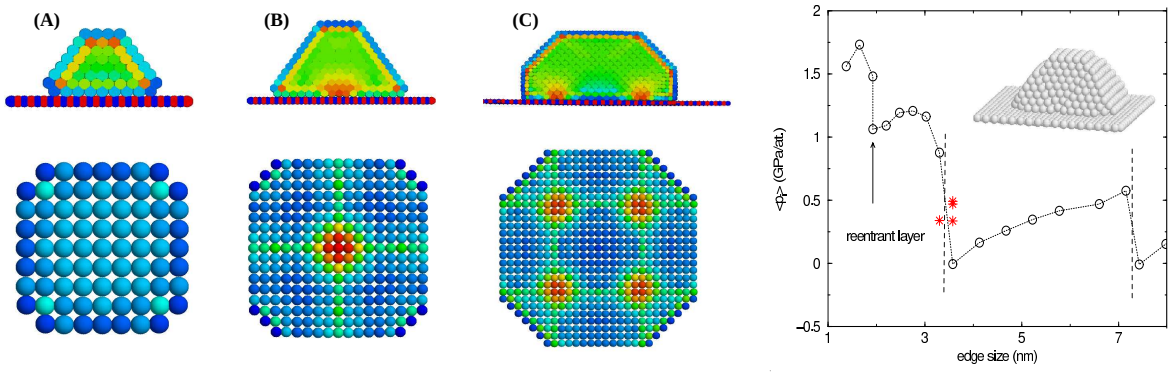

Figure 10: Stress release in supported Pd clusters. Left panel: maps of atomic pressure along a cut perpendicular to the interface (top row), and within the interface Pd layer (bottom row) for clusters of 2.5 (A), 4.7 (B), and 7.4 (C) nm. Red zones correspond to a positive pressure (compression, i.e. negative stress) whereas blue zones correspond to a negative pressure (tension, i.e. positive stress). Intermediate green zones are neutral. Right panel: average stress per cluster and per atom as a function of cluster size. Red stars correspond to clusters whose stress is released via sliding along (111) planes, as depicted in the inset. From [35].

adsorption sites (see the compression zones in Fig. 10 (B)): an interface misfit dislocation is created, which totally releases the strain. As the cluster size further increases, the dislocations organize themselves in a periodic network, leading to a (10x10) superstructure (Fig. 10 (C)), approaching closely the (11x11) incommensurate structure observed at extended Pd/MgO(100) interfaces ($11a_{MgO} \sim 12a_{Pd}$). Stress release by a progressive introduction of the interface misfit dislocations is quantified in the right panel of Fig. 10. An alternative way of partial stress release in small clusters is illustrated in the inset: introduction of (111) sliding planes across the cluster reduces the compression zone around the off-site Pd atomic row and improves the adhesion of smaller prismatic parts at the cluster base. However, since the energy of the sliding plane is proportional to its area, this defect is less energetically favourable in large clusters.

Since at higher metal coverage, the deposited clusters coalesce and a bidimensional layer begins to form, it is interesting to investigate the atomic structure of thin deposited metal films. In particular, Pd and Ag thin films deposited on MgO(100) display interface dislocations similar to those described for the clusters. The dislocation network depends on the lattice misfit: the smaller the misfit, the larger the super-lattice (from 3.3 nm for Pd to 10 nm for Ag). The residual stress, induced by the interface dislocations propagates across the metal film and is at the origin of a nano-structuration of the film's surface, see Fig. 11. As the stress propagates across the metal film, the topology of the local nano-structuration may vary from one atomic layer to another. In the present case of Ag films, in films thicker then ten layers the network of misfit dislocations is recovered on the surface, but the compression and tension zones are inverted. For thinner films (see the intermediate layer in Fig. 11), new tension zones (light blue) appear in the middle of the initial periodic structure and modify its periodicity. Since the elastic strain network acts as a patterning for an adsorbate, a nano-structured metal film may be seen as a promising substrate for the self-organized growth [37].

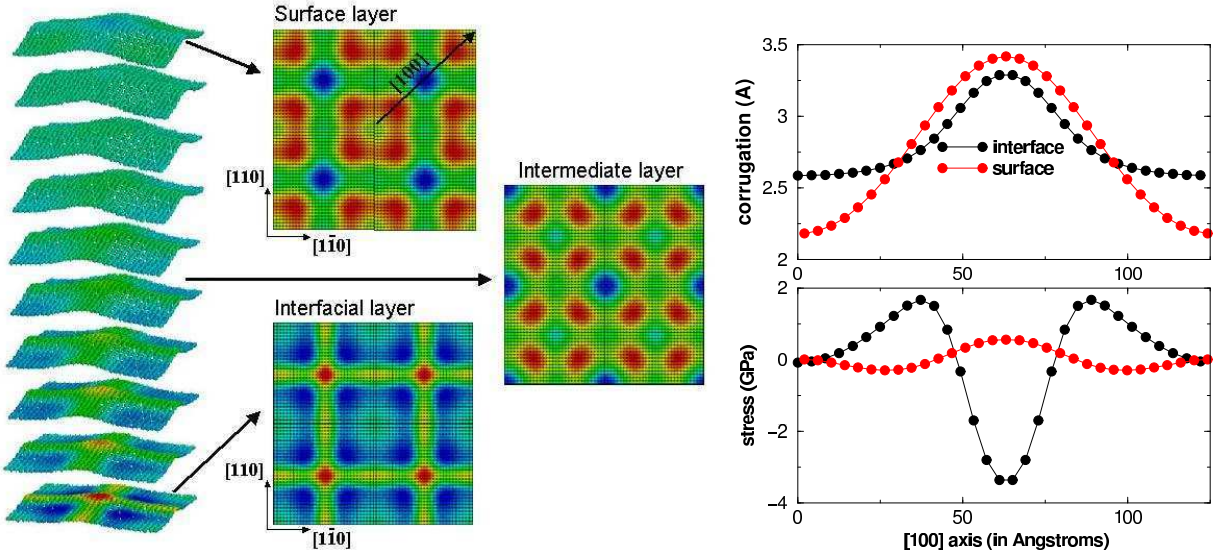

Figure 11: On the left: side view of maps of atomic pressure within the atomic layers of Ag thin film supported on MgO(100) (the same colour code as in Fig. 10): the coordinate perpendicular to the substrate has been dilated artificially as to get a better insight into the corrugation. In the middle: top view of the maps corresponding to surface, interface, and intermediate layer, each on a separate colour scale. Right panel gives the corrugation and the local stress plotted along the [100] direction for the surface and interface Ag layers. From [19].

.

To summarize, the use of model inter-atomic potential derived from first principles calculations permits to take into account all interface degrees of freedom, and to perform an extensive search of minimum-energy structures, without the constraints of pseudomorphic metal/oxide structures. These simulations give access to different mechanisms of strain release in the supported metal clusters of thin films, and enable studies on coupling between the interactions at the interface and the stability and atomic structure of metal deposits.

4 Towards realistic simulations

In the preceding section we have used the results of ab initio calculations on model metal/oxide interfaces as a base of a study on complex metal deposits on the MgO(100) surface. The size of the systems considered in this study and the absence of constrain on the local interface structure bridge two essential aspects separating the experimental reality from results of model calculations. However, several additional ingredients need to be taken into account in order to bring the simulations closer to the reality. In the following we focus on just two of them, chosen because of their qualitatively different character. On one hand, by extending our PES approach described in Sec. 3, we will show a possibility of accounting for the effect of finite temperatures on the properties of deposited clusters. Indeed, since temperature is one of the key factors influencing, eg. different stages of cluster growth and equilibration, it may be seen as an essential ingredient of any realistic simulation. On the other hand, by extending our model ab initio calculations beyond the perfect interfaces described in Sec. 2, we will give examples of

situations in which, due to substrate defects, an otherwise weakly-interacting interface suffers a strong modifications of both electronic and adhesion properties. At present, it is relatively well established that defects determine the characteristics of cluster growth and, potentially, also some of their catalytic properties. Results going beyond the perfect interfaces are thus needed for interpretation of experimentally observed phenomena.

4.1 Finite temperature effects

The main advantage of the PES approach used in the study described in Sec. 3, was to enable an efficient treatment of a large number of structural degrees of freedom (number of independent particles), as to access clusters of "experimental" sizes. Quenched molecular dynamics was employed in those calculations as a tool for an efficient search of equilibrium atomic structures. In the following we present a study which aims an efficient description of oxide-supported metal clusters at finite temperatures. This time, due to atomic vibrations and diffusion, statistical averages need to be calculated in order to quantify cluster properties, and these are the atomic trajectories obtained in molecular dynamics which are used for estimation of various, temperature dependent characteristics and observables. We focus on the melting and re-crystallization of Pd clusters deposited on the MgO(100) surface and analyse the essential substrate-induced characteristics [39].

Since the late transition metals interact weakly with the perfect MgO(100) surface and their cohesive properties are little influenced by the underlying substrate, a prescription for an efficient molecular dynamics simulations is to neglect the complete description of the substrate vibrational degrees of freedom and account for the heat exchange between the substrate and the adsorbate in an effective way. Two different levels of approximation can be conceived. On one hand, the energy exchange between the cluster and the substrate can be ensured by an Andersen thermostat, involving stochastic collisions of interface metal atoms with virtual particles representing the MgO heat bath at fixed temperature. On the other hand, one can use the surface oscillator approach [38], where the motion of the oxide substrate is described through a set of harmonic oscillators of amplitude and frequency derived from ab initio calculations. In the case of our PES model these two methods give equivalent results.

4.1.1 Effect of the oxide substrate on cluster melting

The effect of substrate on the cluster melting and crystallization properties can be deduced from a comparison of caloric curves obtained during heating and cooling of free and supported metal clusters, Fig. 12. The most important effect is the substrate-induced modification of the solid-liquid transition. Both melting (obtained when heating the cluster) and crystallization (obtained when cooling a melted cluster) temperatures increase considerably. The hysteresis (which corresponds to the coexistence loop of the two phases in first order transitions) narrows in the case of deposited clusters and disappears completely at smaller cluster size. The jump of energy representing the latent heat of transition is little affected. The other substrate-induced effect, visible already at relatively low temperatures, is the modification of cluster's morphology. In fact, as soon as diffusion processes are activated, metal clusters deposited in their free equi-

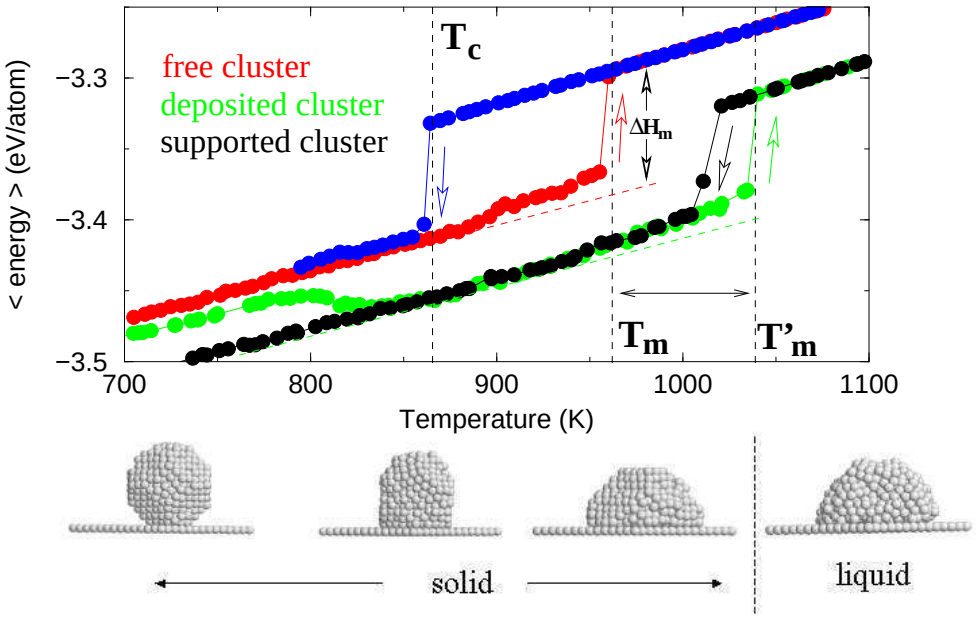

Figure 12: Melting and re-crystallization of a small Pd cluster (about 200 atoms). Top panel gives the caloric curves obtained for free (red), deposited (green), and supported (black) clusters of the same size. Temperature variations (heating and cooling) are indicated with arrows. Latent heat of melting ΔH_m crystallization temperature (T_c), as well as melting temperatures for free (T_m) and deposited (T'_m) clusters are shown. Bottom panel gives the series of snapshots of the deposited cluster atomic structure taken at temperatures below and above T'_m. From [39].

librium shape (first snapshot in the bottom panel of Fig. 12) distort progressively as to adopt their supported equilibrium shape on the MgO(100) surface (third snapshot in the bottom panel of Fig. 12).

4.1.2 Surface premelting and dependence on the cluster size.

The maps of averaged structural characteristics (position, mobility) taken at different temperatures along the caloric curve, Fig. 13, help visualizing the process of cluster melting. The atoms which diffuse at the lowest temperatures are the lowest coordinated ones (at the edge of re-entering layer at the interface). As temperature is progressively increased, more and more atoms, first at cluster edges, than at its (100) top facet, and finally at its (111) side facets become mobile. This formation of a thin liquid layer in equilibrium with the underlying solid core (surface premelting), starts at temperatures well below the actual solid-liquid transition and disappears for very small cluster sizes (where there are practically no core atoms). In the present case of supported Pd clusters, the surface premelting clearly does not involve the metal atoms at the interface, whose mobility is systematically close to that of cluster core sites. However, since the mobility properties of metal atoms directly at the interface depend on the strength of the metal-oxide interaction they are expected to approach those of the metal itself at weakly interacting interfaces.

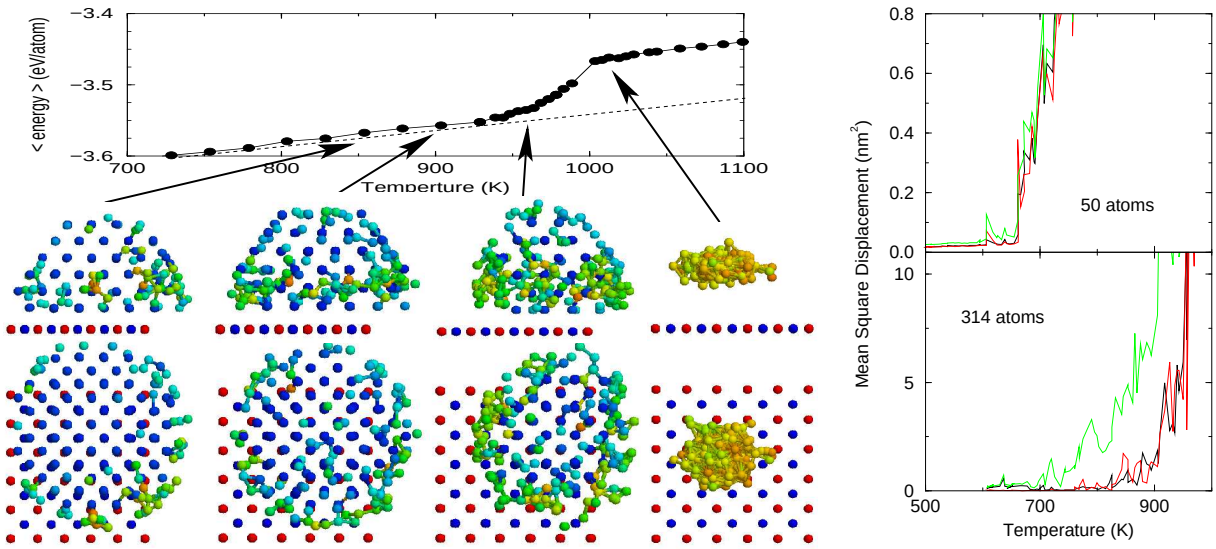

Figure 13: Melting of supported Pd clusters. Left panel presents a series of images of a progressively heated cluster: metal atoms are plotted at their average atomic positions, their colours represent their mean square displacement. Colour scale ranges from dark blue (immobile), through green, to yellow and red (highly mobile). Right panel displays the evolution of the mean square displacement as a function of temperature for three types of Pd atoms in the supported cluster: core (black), interface (red), and surface (green). Small (50 atoms) and medium size (314 atoms) clusters are considered. From [39].

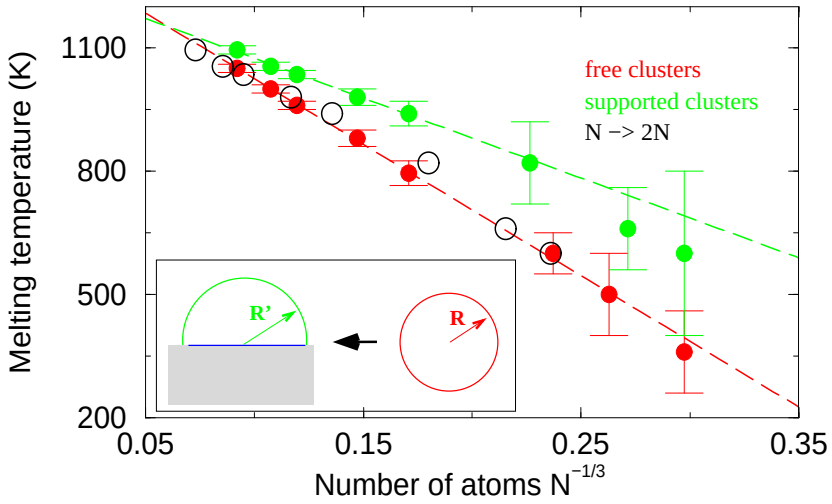

Figure 14: Substrate-induced modifications of the melting temperature of supported Pd clusters. Melting temperature as a function of cluster size (inverse cluster radius $N^{-1/3} \sim R^{-1}$) for free (red) and supported (green) clusters. Black circles represent the melting temperature of supported clusters corrected for the modification of the surface/volume ratio (see text). The inset displays a schematic representation of substrate-induced modification of equilibrium form of Pd clusters: perfectly spherical free shape (red) and half-spherical supported shape (green). From [39].

4.1.3 Interface-induced delay of melting

In order to relate the observed absence of premelting at the Pd/MgO(100) interface to the substrate-induced modification of the melting temperature of the deposited clusters we use the phenomenological law of Gibbs-Thompson. It gives the general relation between the melting temperature T_m of a given cluster and its size (radius R): $T_m(R) \sim -R^{-1}$, and accounts for the well known effect of reduction of the melting temperature in spherical particles of finite size. Indeed, for both free and supported clusters we find a linear variation of melting temperature as a function of inverse cluster radius ($R^{-1} \sim N^{-1/3}$), Fig. 14. Higher melting temperatures in the case of supported clusters gives somewhat smaller proportionality constant. In order to access the mechanism underlying this difference we remind that this is the surface ($\sim R^2$) to volume ($\sim R^3$) ratio which is at the origin of the R^{-1} argument in the Gibbs-Thompson law.

Upon the cluster deposition two effects are to be taken into account. On one hand, the cluster morphology changes and the overall cluster surface increases. On the other hand, depending on the strength of interactions on the metal/substrate interface, the extent of premelting in the interfacial metal layer varies. In the present case of Pd clusters on the MgO(100) surface, the deposition-induced change of cluster shape (full sphere into half sphere, inset of Fig. 14) reinforces the surface/volume ratio. However, since the interface atoms do not show any premelting, only the external cluster facets act as melting precursors. As a consequence the effective surface diminishes by $2^{-1/3}$, and so does the surface/ratio entering the Gibbs-Thompson equation. The corresponding transformation does align the melting temperatures of supported and free clusters, Fig. 14. It emphasis that it is the interface-induced reduction of premelting rather than to the change of cluster morphology which is responsible for the calculated delay of melting.

Although the present results on Pd clusters deposited on the MgO(100) surface present a very particular scenario of cluster melting, they reveal the principal underlying mechanisms which give basis for a more general conclusion. Whereas at weaker interacting interfaces, the properties of deposited clusters shall approach these of the free ones, in the case of strong interaction at the interface one may expect a delay of melting of the interface layer with respect to the cluster core, giving potentially rise to an interesting case of interface "post-melting".

4.2 Substrate polarity and the role of point defects

Any attempt to simulate realistic metal/oxide interfaces has to take into account the possibility of structural, chemical, or electronic defects, stabilized either by the specific metal/oxide environment, or by the conditions of sample preparation. Especially as regards the characteristics of metal growth, the substrate defects are widely recognized to play an essential role. Their characterization and the analysis of their influence on the initial stages of nucleation has recently become a subject of extensive theoretical and experimental studies. Much less is know on the role of defects in the catalytic properties of supported metal nano-clusters. In the following, we focus our attention on the influence of substrate defects on the properties of constituted interfaces. We have chosen two qualitatively different cases: an interface with a polar, or with an oxygen deficient oxide surface, representative respectively, for model extended and point defects. Although their physical origin is very different, both these kinds of defects are responsible for

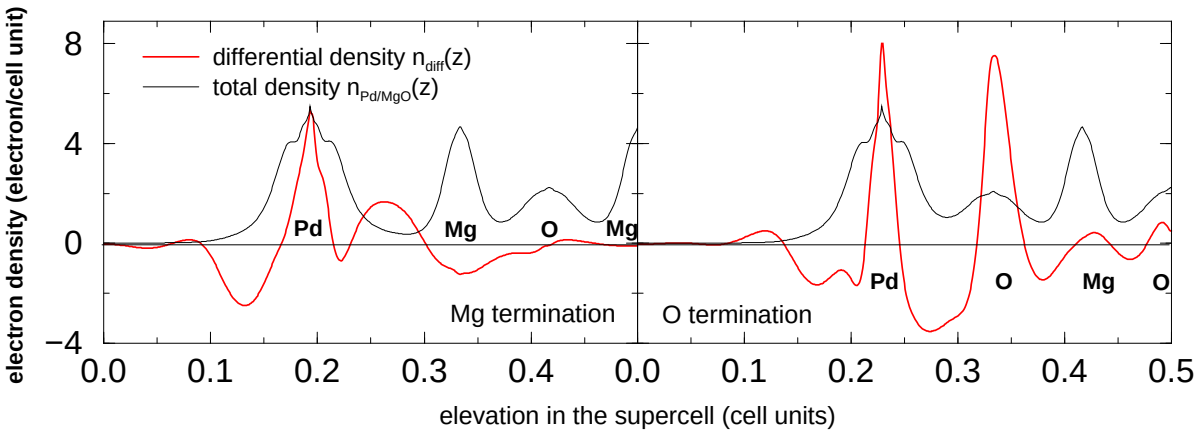

Figure 15: Electron redistribution upon deposition of a Pd layer on the two terminations of MgO(111) surface. Red lines represent profiles of differential electron density across the interface $n_{\text{diff}}(z) = n_{\text{Pd/MgO}}(z) - n_{\text{Pd}}(z) - n_{\text{MgO}}(z)$. Black lines give the (scaled) total electronic density $n_{\text{Pd/MgO}}(z)$, whose maxima indicate the positions of the atomic layers in the supercell. From [20].

important modifications of the interface electronic structure. Even in the case of metals from the end of the transition series, they are at the origin of a strong interaction at the interface.

4.2.1 Polar metal-oxide interfaces

The problematics of metal/oxide interface gains an additional dimension in the case of polar orientations of the substrate surface. Although polar oxide surfaces are well recognized to be unstable and thus difficult to prepare unreconstructed and defect-free [40, 41, 42, 43, 44, 45], there exists both experimental and theoretical evidence that formation of a metal/oxide interface can stabilize polar oxide terminations [46, 47, 48].

Indeed, a simple electrostatic argument explains the instability of polar oxide surfaces, such as the MgO(111) one, and suggests how they can be stabilized. The presence of equidistant layers, with charge densities equal alternatively to $+\sigma$ and $-\sigma$ yields a macroscopic dipole moment which increases with the number of layers. This divergent component can be cancelled out by the introduction of additional (compensating) charge densities $\mp\sigma/2$ on the outer layers of the slab. Various mechanisms leading to this compensation at the MgO (111) surface were described in the literature, among which non-stoichiometric reconstructions [49] and hydroxylation [49, 50]. Adsorption of metals is an equally efficient way of stabilizing of the MgO(111) surface [20].

The metal adsorption characteristics on MgO(111) are controlled by its strong polar character and thus differ substantially from those reported for the MgO (100) face. In particular, strong electron transfers between the metal atoms and the substrate take place, resulting in a strong interface adhesion.

We recall that on the clean MgO (111) substrate, the condition of polarity healing is fulfilled thanks to a modification of the surface valence and conduction band filling: on the oxygen (magnesium) termination, the valence (conduction) band is partly depleted (filled). This leads to a

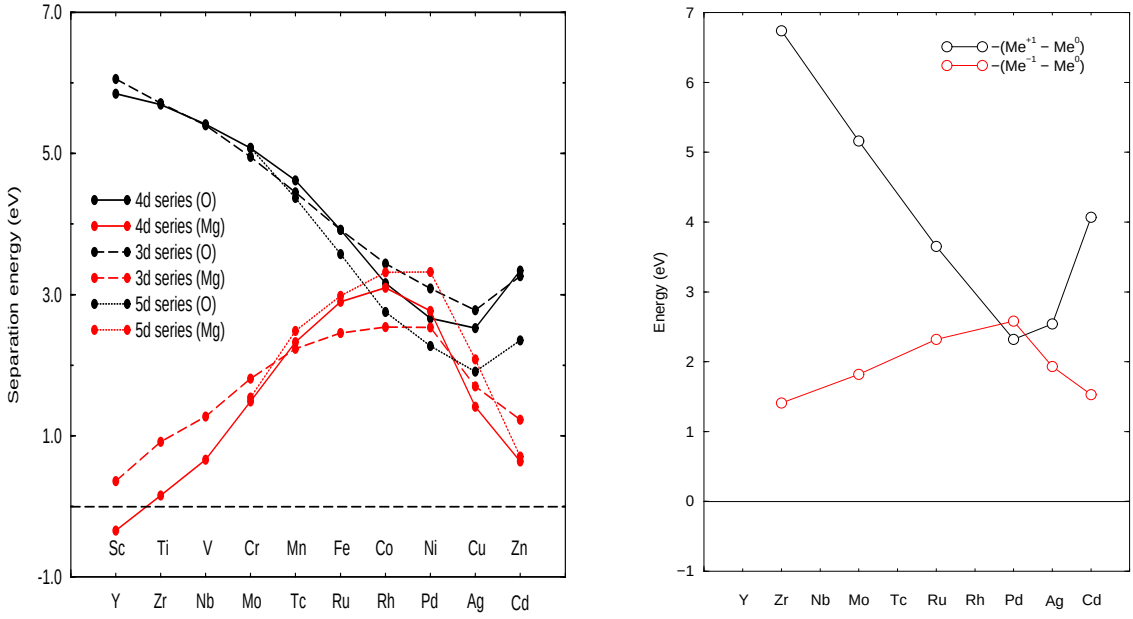

Figure 16: Adhesion at polar metal/oxide interface. Left panel: separation energy (eV/interface metal atom) for a single transition metal layer deposited on oxygen (black) or magnesium (red) termination of the MgO(111) surface (FP-LMTO calculations). Right panel: Energy (eV/atom) required to positively or negatively ionize an unsupported strained metal layer (*4d* transition series, FP-LAPW calculations). Only the evolution is meaningful. Since this energy represents the metallic band filling contribution to $E_{\rm sep}$, global shifts have been made to align the curves with the separation energy curves (left panel). From [20].

reduction (in absolute value) of the surface charges and to a metallization of the two terminations. We have shown in Ref. [48] that this mechanism yields charge compensation but results in a high surface energy. When a metal layer is deposited on the MgO(111) surface we find a completely different situation. The substrate bands recover a normal filling and the metal band filling changes. The metal overlayer gives electrons to the MgO surface oxygen (oxygen termination) and receives electrons from the MgO surface magnesium (magnesium termination), in such a way that electrostatic criterion is fulfilled, Fig. 15. Thus, on metal/MgO(111) interfaces, the compensating state is mainly localized at the adsorbed metal interface layer. The fact that the electronic density of the second and following metal layers remain practically unchanged is a manifestation of strong screening effects present in metallic systems.

The evolution of separation energies at metal/MgO(111) interfaces along the transition series, Fig. 16, is driven by the contribution associated to the transfer of the compensating state from the substrate towards the metal. It induces an energy gain (positive contribution to $E_{\rm sep}$), function of the relative positions of the magnesium, oxygen, and metal bands on the energy scale. It can be qualitatively estimated by the energy required to charge positively or negatively all atoms in an unsupported strained metal layer. As shown in Fig. 16, this contribution accounts for the principal characteristics of the $E_{\rm sep}$ behaviour along the transition series. Although the behaviours of metal/MgO(111) and metal/MgO(100) (Fig. 5) separation energies along the transition series present an overall similarity, the separation energies at metal/MgO(100) interfaces are systematically smaller. The difference is due to different surface energies of the

clean MgO(111) and MgO(100) surfaces and amounts to about 2.1 eV/surface MgO unit. Since the separation energy of metal on the MgO (111) surface is high (the adsorption process stabilizes significantly the polar surface), an estimation of the contact angle θ through the Young-Dupré equation ($E_{sep} = \gamma(1 + \cos\theta)$, where γ is the energy of metal surface), for metals at the end of transition series we find the possibility of total wetting ($\theta = 0$) of the unreconstructed (111) surface by the deposit, whereas bad wetting ($\pi/2 < \theta < \pi$) is found for the (100) orientation.

In summary, the interaction of transition metal with a polar surface of a highly ionic oxide is dominated by the band filling modification which is necessary for suppressing the macroscopic dipole moment in the polar substrate. Transfer of the compensating state from the substrate to the adsorbed metal results in a strong energy gain which enhances thus the adhesion at the interface. As a consequence, the very same transition metal may interact weakly with non-polar faces of a given oxide and wet perfectly the polar ones.

4.2.2 Palladium on oxygen deficient MgO(100) surface

The improvement of experimental techniques enables a better characterization of surface point defects, of their effect on the interaction between oxide substrate and the adsorbate, and finally, of their influence on chemical activity of metal deposits [51]. On one hand, Atomic Force Microscopy experiments have shown that the nucleation kinetics is governed by point defects with a high trapping energy [52]. Also the peculiar catalytic properties of supported clusters have been tentatively attributed to defect-induced modification of the electronic properties of the deposited metal [53]. On the other hand, it has recently been show that in oxygen-poor (UHV) conditions, the surface oxygen vacancies - probably the most widely studied point defects on MgO(100) - are thermodynamically more stable than magnesium or di-vacancies (missing surface MgO units) [54]. The theoretical studies reveal also an important increase of the adsorption energy of metal ad-atoms and a considerable electron transfer induced by oxygen vacancies [55, 56, 57, 58, 59, 16, 60]. Whereas most of results concerns the isolated metal ad-atoms, dimers, or nano-clusters composed of a few atoms only, and are thus representative of the very early stages of cluster growth, in the following we focus on the effect of oxygen vacancies on electronic and adhesion properties of extended metal deposit (Pd/MgO(100) interface).

We recall that the most stable, neutral oxygen vacancies, are characterized by trapping of two electrons by the surface electrostatic field on the site of the missing oxygen atom and by the existence of an occupied state in the MgO band gap. Compared to metal deposition on the defect-free MgO(100) surface, they are responsible for an enhanced electron transfer from the substrate towards the deposit. The transferred electrons remain well localized on the metal atom directly above the vacancy site, which also receives some electrons from its metal neighbours. This electron redistribution can be correlated to the relative position of the vacancy state and the metal band on the energy scale, but the band shift and deformation due to the electron transfer needs to be taken into account self-consistently. In the case of Pd/MgO(100) interface, the LDOS of Pd atom directly above the vacancy is shifted downwards on the energy scale, and its width is considerably reduced, Fig. 17. The electronic population at this atom is enhanced, but the reduced LDOS width reflects a high degree of localization of the transferred electrons. In view of this result on may expect that the enhanced catalytic activity suggested for isolated

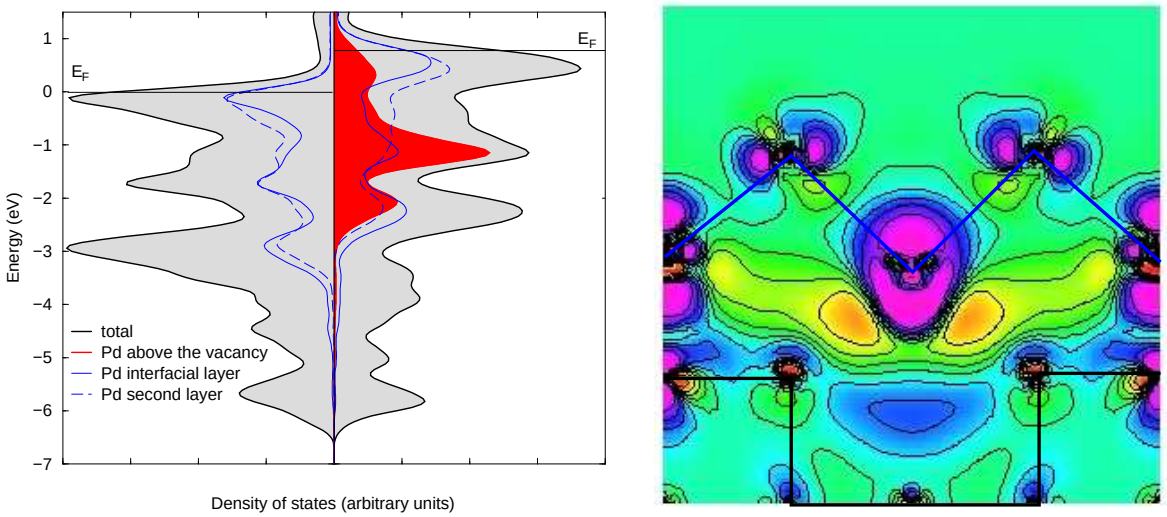

Figure 17: Palladium bi-layer deposited on the oxygen-deficient MgO(100) surface (0.25 ML of neutral oxygen vacancies). Left panel: local density of states calculated for Pd deposited on perfect (left column) and oxygen deficient (right column) surface. Projections on the Pd atoms above the vacancy (red), in the interface layer (solid blue), and in the second layer (dashed blue) are plotted. The energy scales are aligned by the core levels of oxygen ions in the slab center. Right panel presents the map of differential electron density in the plane perpendicular to the interface, and centered on the Pd atom above the vacancy. Black (blue) line interconnects substrate (adsorbate) atoms. Colours yellow and red correspond to an enhancement of electron density, whereas blue and violet represent a reduction. From [16].

metal ad-atoms trapped at oxygen vacancies [58], may also exist for extremely flat clusters or at the edges and corners of three dimensional clusters deposited of defected surface. However, similarly to the case of polar interfaces, the electronic redistribution remains fairly localized to the interface region and is likely to be completely screened in larger three-dimensional deposits.

Due to the stabilizing effect of the electron transfer just described, oxygen vacancies enhance considerably the adhesion energy. Although, compared to adsorption of isolated metal atoms, their effect attenuates rapidly for more extended deposits, and remains much smaller than this of a polar substrate, oxygen vacancies may yield a modification of the aspect ratio of deposited particles. A simple argument based on the Wulff theorem and applied to the known, pyramidal form of Pd clusters on MgO(100) suggests a reduction of the cluster height and thus an increase of the proportion of (100) facets with respect to (111) ones. This effect, together with the related change of edge lengths will necessarily modify the cluster catalytic properties. Although the controlled generation of surface defects may seem to be a tool for a fine tuning of catalyst reactivity, one should not forget that the presence of vacancies may also induce structural defects within the deposit, modify the kinetics of cluster growth, and the cluster size distribution.

5 Conclusion

We have proposed a novel approach to simulation weakly interacting metal/oxide interfaces which couples the advantage to relay on results of model ab initio calculations (and to account

thus for the many-body character of the interactions), with the efficiency of PES-type methods. We have given an example of its application to a study on oxide-supported metal clusters and thin metal films, and have shown the possibility to perform finite temperature simulations at a relatively small computational expense. Both, the large number of treated atoms, and the account of temperature, do unquestionably approach the realistic experimental conditions. In the particular case of the described systems, this two ingredients have helped to reveal physical effects which at present are clearly beyond the reach of ab initio calculations.

We have also introduced the substrate defects - an another factor which often determines the observed characteristics and is responsible for the most interesting properties. The two qualitatively different examples (a polar and an oxygen-deficient substrate surface) reveal an enhanced electron transfer and adhesion energy, which are inherent of most substrate defects. Corresponding modifications of the properties of deposited metal may complicate any possible extension of the PES method towards this kind of interfaces but, at present, more model ab initio results are still necessary in order to rationalize the apparently complex behaviour of metals on defected oxide surfaces.

References

[1] R. Car and M. Parrinello, Phys. Rev. Lett. (1985).

[2] V. E. Henrich and P. A. Cox, *The Surface Science of Metal Oxides* (Cambridge University Press, Cambridge, 1994).

[3] C. Noguera, *Physics and Chemistry at Oxide Surfaces* (Cambrige University Press, Cambridge, 1995).

[4] M. W. Finnis, J. Phys.: Condens. Matter **8**, 5811 (1996).

[5] F. Didier and J. Jupille, Surf. Sci. **314**, 378 (1994).

[6] H. J. Freund, H. Kuhlenbeck, and V. Staemmler, Rep. Prog. Phys. **59**, 283 (1996).

[7] G. Renaud, Surf. Sci. Rep. **32**, 1 (1998).

[8] C.R. Henry, Surf. Sci. Rep. **31**, 231 (1998)

[9] M. Methfessel, Phys. Rev. B **38**, 1537 (1988); M. Methfessel, C. O. Rodriguez, and O. K. Andersen, Phys. Rev. B **40**, 2009 (1989).

[10] P. Blaha, K. Schwarz, and J. Luitz, WIEN97, Vienna University of Technology 1997. (Improved and updated Unix version of the original copyrighted WIEN-code, which was published by P. Blaha, K. Schwarz, P. Sorantin, and S.B. Trickey, Comput. Phys. Commun. **59**, 399 (1990)).

[11] J. P. Perdew, K. Burke, and Y. Wang, Phys. Rev. B **54**, 16533 (1996).

[12] J. Goniakowski, Phys. Rev. B **57**, 1935 (1998).

[13] J. Goniakowski, Phys. Rev. B **59**, 11047 (1999).

[14] J. Goniakowski and C. Noguera, Interf. Sci. **12** 93 (2004).

[15] G. Bordier and C. Noguera, Phys. Rev. B **44**, 6361 (1991).

[16] L. Giordano, J. Goniakowski, G. Pacchioni, Phys. Rev. B **64**, 075417 (2001).

[17] J. Goniakowski, Phys. Rev. B **58**, 1189 (1998).

[18] D. Fuks, S. Dorfman, Yu F. Zhukovskii, E. A. Kotomin, and A. M. Stoneham, Surf. Sci. **499**, 24 (2002).

[19] A. Ouahab, C. Mottet, and J. Goniakowski, to be published.

[20] J. Goniakowski, C. Noguera, Phys. Rev. B **66**, 085417 (2002).

[21] K. Yamamoto, Y. Kasukabe, R. Takeishi, and T. Osaka, J. Vac. Sci. Technol. A **14**, 327 (1996).

[22] R. Yamauchi, M. Kubo, A. Miyamoto, R. Vetrivel, and E. Broclawik, J. Phys. Chem. B **102**, 795 (1998).

[23] R. Benedek, A. Alavi, D. N. Seidman, L. H. Yang, D. A. Muller, and C. Woodward, Phys. Rev. Lett. **84**, 3362 (2000).

[24] J. Oviedo, J. Fernández Sanz, N. López, and F. Illas, J. Phys. Chem. B **4**, 4342 (2000).

[25] W. Vervisch, C. Mottet, and J. Goniakowski, Phys. Rev. B **65**, 245411 (2002).

[26] J. Friedel, The Physics of Metals, ed. J.M. Ziman (Cambridge University Press, 1969).

[27] S. Sawaya, J. Goniakowski, C. Mottet, A. Saúl, and G. Tréglia, Phys. Rev. B **56**, 12161 (1997).

[28] F. Ducastelle, J. Phys., Paris, **31**, 1055 (1970).

[29] V.Rosato, M.Guillopé, and B.Legrand, Phil. Mag. A **59**, 321 (1989).

[30] J. L. Rousset, A.M. Cadrot, F.J. Cadete Santos Aires, A. Renouprez, P. Mélinon, and A. Perez, J. Chem. Phys. **102**, 8574 (1995).

[31] J. Guevara, A.M. Llois, and M. Weissmann, Phys. Rev. B **52**, 11509 (1995).

[32] C. Mottet, G. Tréglia, B. Legrand, Surf. Sci. **352-354**, 675 (1996).

[33] F. Baletto R. Ferrando, A. Fortunelli, F. Montalenti, C. Mottet, J. Chem. Phys. **116**, 3856 (2002).

[34] C. Mottet, J. Goniakowski, F. Baletto, R. Ferrando, and G. Tréglia, Phase Transitions, **77**, 101 (2004).

[35] W. Vervisch, C. Mottet, and J. Goniakowski, Eur. Phys. J. D **24**, 311 (2003).

[36] H. Graoui, S. Giorgio, and C.R. Henry, Phil. Mag. B **81** , 1649 (2001).

[37] H. Brune, M. Giovani, K. Bromann, and K. Kern, Nature **394**, 451 (1998).

[38] H.F. Busnengo, W. Dong, P. Sautet, and A. Salin, Phys. Rev. Lett. **87**, 127601 (2001).

[39] C. Mottet and J. Goniakowski, Surf. Sci., in press (2004).

[40] N. Floquet and L. C. Dufour, Surf. Sci. **126**, 543 (1983).

[41] V. E. Henrich, Surf. Sci. **57**, 385 (1976).

[42] H. Onishi, C. Egawa, T. Aruga and Y. Iwasawa, Surf. Sci. **191**, 479 (1987).

[43] R. Plass, K. Egan, C. Collazo-Davila, D. Grozea, E. Landree, L. D. Marks, and M. Gajdardziska-Josifovska, Phys. Rev. Lett. **81**, 4891 (1998).

[44] P. A. Cox and A. A. William, Surf. Sci. **152/153**, 791 (1985).

[45] C. Noguera, J. Phys. : Cond. Matt. **12** R367, (2000).

[46] D. Imhoff, S. Laurent, C. Colliex, and M. Backhaus-Ricoult, Eur. Phys. J. AP **5**, 9 (1999).

[47] R. Benedek, M. Minkoff, and L. H. Yang, Phys. Rev. B **54**, 7697 (1996).

[48] J. Goniakowski and C. Noguera, Phys. Rev. B **60**, 16120 (1999).

[49] A. Pojani, F. Finocchi, J. Goniakowski, and C. Noguera, Surf. Sci. **387**, 354 (1997).

[50] K. Refson, R. A. Wogelius, D. G. Fraser, M. C. Payne, H. Lee, and V. Milman, Phys. Rev. B **52**, 10823 (1995).

[51] C. Barth and C.R. Henry, Phys. Rev. Lett. **91**, 196102 (2003).

[52] G. Haas, A. Menck, H. Brune, J.V. Barth, J.A. Venables, and K. Kern, Phys. Rev. B. **61**, 11105 (2000).

[53] A. Sanchez, S. Abbet, U. Heiz, W. D. Schneider, H. Häkkinen, R. N. Barnett, and U. Landmann, J. Phys. Chem. A **103**, 9573 (1999).

[54] B. Ealet, J. Goniakowski, and F. Finocchi, Phys. Rev. B in press (2004).

[55] A. M. Ferrari and G. Pacchioni, J. Phys. Chem. **100**, 9032 (1996).

[56] A.V. Matveev, K.M. Neyman, I.V. Yudanov, and N. Rösch, Surf. Sci. **426**, 123 (1999).

[57] A. Bogicevic, D.R. Jennison, Surf. Sci. **437**, L741 (1999).

[58] S. Abbet, A. Sanchez, U. Heiz, W. -D. Schneider, A. M. Ferrari, G. Pacchioni, and N. Rösch, J. Am. Chem. Soc. **122**, 3453 (2000).

[59] Yu F. Zhukovskii, E. A. Kotomin, P. W. M. Jacobs, A. M. Stoneham, and J. H. Harding, J. Phys.: Condens. Matter **12**, 55 (2000).

[60] L. Giordano, C. Di Valentin, J. Goniakowski, and G. Pacchioni, Phys. Rev. Lett. **92**, 096105 (2004).